International Journal of
INTELLIGENT SYSTEMS AND APPLICATIONS IN ENGINEERING

ISSN:2147-6799 www.ijisae.org Original Research Paper

Recognition of Injury for Diabetic Retinopathy by using Texture Descriptors

R. Sujitha*[1], Subhajini A.C[2]

Submitted: 10/09/2022 **Accepted:** 20/12/2022

Abstract: Diabetic retinopathy and diabetes hyperglycemia are becoming more common over the global. Presently, otolaryngologists are having a difficult time distinguishing between the different phases of eye problems. Microaneurysm is the first step of such phases. A new texture-based machine microaneurysm diagnosis technique is described. The textured descriptive show that participants the textural properties of every picture, greatly increasing MA detection capability over pattern characteristics. When applying a Logistic regression classifier to differentiate the tumors, the retrieved characteristics from the Local Binary Pattern contributes significantly. The suggested project schedule is depicted in Figure 1 and contains six phases: (1) spatial measurement, (2) preprocessing, (3) optic region, (od) elimination, (4) candidate retrieval, (5) extraction of features, and (6) categorization. The output of proposed is simulated in matlab and compared with existing approaches, proposed it performs better than the existing methodologies.

Keywords: *Diabetic retinopathy, Local binary pattern, Microaneurysms, Circular Hough transform.*

1. Introduction

As per International Diabetes Federation (IDF), around 366 million individuals worldwide identified as mellitus in 2011, even with number anticipated to rise to 522 billion in 2030 [1]. Nearly every day, four million people get eye diagnostic tests as a result of the massive increase in mellitus patients across the country. Diabetic retinopathy (DR) is one of the five primary causes of impaired vision, according to epidemiology research. Non-proliferative diabetic retinopathy (NPDR) and progressive diabetic retinopathy (PDR) are really the two primary stages of DR (PDR). The enlargement of microscopic blood arteries designated microaneurysms is a sign of NPDR in its initial phases (MAs). Red blemishes are another name for MAs. The arteries also degenerate, as well as the leaking causes bleeding, which is characterised by little red spots.

A next step is tough opac, in which microscopic, blood smear capillaries in the retinal close, resulting in merino speckles known as wet cotton blotches. Circulatory issues and respiratory failure develop in the PDR stage, resulting in artery destruction and retinopathy [2]. In order to aid optometrists in the identification of MAs, automatic identification techniques now are recommended [3]. As a result, human mistakes can be minimized. DR identification is a very well area of investigation wherein investigators concentrate their efforts and give innovative thoughts to advance multiple analytical methodologies.

As a result, investigators offered numerous detection approaches in the identification of MAs, taking into account limited capability, exorbitant prices, and intellect. A system for categorising MAs in lesion pictures was established by Fleming et al. [4]. The image is converted before being processed including 3 average and Stochastic filters. The reddish patches are detected using the K-nearest neighbour classification, that has a responsiveness of 85.4 percent and a consistency of 83.1 percent. A cross correlated processing strategy was used in [5] can identify every reddish tumours in panchromatic photographs. The free-response operating characteristic (FROC) value of 0.201 is reached whenever this strategy is evaluated using the ROC sample. Furthermore, [6] proposed a method in which a retinal picture is obtained with a dual filtering and 28 characteristics are chosen utilizing hierarchical clustering. The collected model was trained a convolutional neural network to identify MAs, with just a sensibility of 68 percent for the ROC collection. In [7] described a technique for detecting MAs automatically. MAs are classified using a recurrent neural network backpropagation classifier that extracts template matching characteristics first from image pixels. The results are compared to two publicly available datasets: diaretdB0 and DIARETDB1. For diaretdB0, the responsiveness, selectivity, and accurateness are 98.32 percent, 97.59 percent, and 97.86 percent, correspondingly, whilst for DIARETDB1, the achievement verifications are 98.91 percent, 97.65 percent, and 98.33 percent. Moreover, in [8], MA identification is performed using a novel approach that preprocesses the incoming optic picture and extracts characteristics by using underside inversion. Genuine MA infections are diagnosed using hierarchical clustering after the plasma arteries are segregated. The ROC subset was examined and found to have a responsiveness of 88.06 percent, a concreteness of 97.47 percent, and a precision of 92 percent. Furthermore, [9] suggested a strategy for classifying MAs which can be done in 3 phases. The very first phase is preparation, which involves applying Gaussian screening and an adjustable distribution to a color image of such optic disc. The MA contender is retrieved in the two stages that use the Gaussian linear regression approach. Ultimately, MAs are categorised that used the KNN classifier, having 96.3 percent sensitivities and 88.4 percent accuracy based on the ROC sample. Furthermore, [10] described a 2 different approach for detecting MAs. During scaling, the preprocessing is done with data augmentation in stage I. Finally, using simple regression recurrent segmentation, characteristics are obtained. To train and retrieve the outcome in stage 2, a realistic assumptions convolution neural network (CNN) is used. The method was implemented also with DIARETDB1 dataset and

[1] *Research Scholar, Department of Computer Applications, Noorul Islam Centre for Higher Education, Kanyakumari, Tamilnadu, India.*
[2] *Associate Professor, Department of Computer Applications, Noorul Islam Centre for Higher Education, Kanyakumari, Tamilnadu, India.*
** Corresponding Author Email: sujithar.mca@gmail.com*

obtained 96.1 percent accurateness. [11] described a multiple CNN approach for detecting MAs, wherein the picture is preprocessed utilizing threshold method. The picture fragments are retrieved during the candidate's separation process, and then CNN is utilised to train and distinguish MAs against non-MAs. In the ROC sample, participants got a FROC result of 0.461. Despite the greater effectiveness, manually learning of model parameters using the investigation approach reduces computing time. In furthermore, [12] described a new approach for detecting MAs termed stacking patchy classifier.

The picture chunks are used to capture elevated characteristics that are then utilised to classify images, increasing the platform's complexities. The curve (AUC) again for squishy classification is 0.913, but for the F-measure predictor, it is 0.962. The researchers in the preceding literature alluded to the difficulty and complication of categorising MAs. As a consequence, the disadvantages are as follows: I the use of huge datasets require high computational power required to train, (ii) the convolution layer in the system increase the difficulty, and (iii) the outcomes are hard to decipher. The computational cost exponentially with the number of units within network grows. Furthermore, the improvement is insignificant. In [13] implements an automatic MA identification utilising dense PCA-based classification, with a FROC value of 0.275. The sparse representation classification (SRC) is frequently used in frame buffer assessment and has shown to generate improved results [14]. Despite this, there are a few flaws in this SRC approach for MA identification. Because SRC utilizes unprocessed training photos, the retina input images have non-uniform brightness and turbulence, reducing the MA categorization effectiveness and stability of the system. In contrast, pattern characteristics were preferred, that were dependent on the precision of the candidate's categorization. Due to the limited brightness of retina pictures, obtaining accurate results during the preprocessing step is problematic. For its consistency and multi resolution characterization, a crispness methodology is inferred in our methodology to solve these issues. The distribution of the MA segmentation stage and blood clot sector is generated using the local binary pattern (LBP) approach for texture analysis. To distinguish MA infections from these other alterations such as bloodstream, DR categories, and ambient noise, the supervised classifier is used. The following is how the rest of this article is organized: Part 2 delves deeper into the suggested MA detection approach. The analysis and conversation are presented in Part 3. Part 4 contains conclusion and future recommendations for the suggested work.

2. Proposed Tactic

The suggested project schedule is depicted in Figure 1 and contains six phases: (1) spatial measurement, (2) preprocessing, (3) optic region, (od) elimination, (4) candidate retrieval, (5) extraction of features, and (6) categorization. The suggested system is detailed in depth in the subcategories that follow.

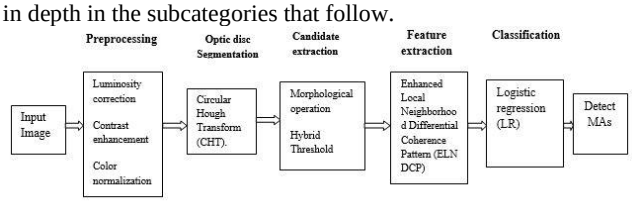

Figure 1. Design of the proposed methodology

2.1. Spatial Measurement

Prior to beginning the preprocessing phase, spatial measurements are required on the obtained input optic picture. As a result, spatial measurement is added in [15] to accommodate varied dimensions. Rather than scaling the picture, the dimension consistent factor is the radius (R) of the complete image. The optic picture is generally taken with a FOV of 45° throughout DR study. In Equation (1), the denominator of d1, d2, and d3 remained the same whether the FOV is changed. The radius 'R' is selected as the kernel function of several filtration in our strategy. In the preprocessing phase, three sets of factors are considered to create the filtration:

$d1= 2R/10, d2=2R/360, d3=2R/30$ (1)

2.2. Preprocessing

2.2.1. Correcting the lighting

The lighting adjustment approach, which is previously mentioned in [15], is chosen to achieve luminance across the picture. Equation (2) reveals the procedure:

$I_a=I+s-I*m_1$

where m_1 is a huge mean filter with a diameter of d1 and s is the source picture's average brightness.

2.2.2. Noise reduction

Noise anomalies can arise throughout image capture and encoding. Complicated and misinterpretation results while decoding a picture which containing noises. As a result, Eq. (3) may be used to create a de-noised picture I_n:

$I_n=I \pm \omega - I_a * m_2$ (2)

where m_2 is a tiny mean filtering with dimension d2 and is the average of pixel intensities.

2.2.3. Brightness Equalization with Adjustable Brightness

After Noise reduction, the brightness equalisation phase is important. The square root of variations at every color image, referred to as localized standard deviation, could be used to assess brightness fluctuation (I_{BF}). The reduced sections are now enhanced with the interpretation:

$I_{ac}= I_n+\{1/ I_{BF}\}*[I_n*(1-m_3)]$ (4)

where m_3 is an elevated filter for obtaining the reduced parts.

2.2.4. Normalization of colour

Color normalisation is necessary after brightness equalisation to create a standardised colour image. For standardising the colour in the especially in comparison image ' I_{ac},' the mean (σ) and standard deviation (σ) are calculated. To eliminate the undesirable edges of every stream element of 'I_{ac},' the display approach is used. Inside a region of ω±3σ, it is normalised by employing stochastic extending and cropping procedures, and the resultant precompiled photos are displayed in Figure 2.

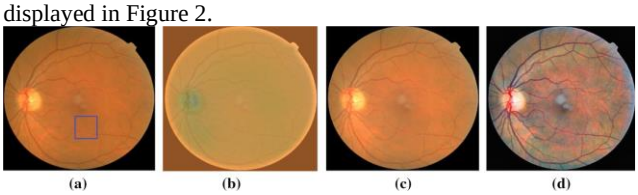

Figure. 2 Phases in pre-processing: a) original picture, b) Brightness leveling, c) Adaptive dissimilarity leveling, d) Shade regularization

2.3. Disposal of the optic disc

To prevent wrong positives identification of MA tumours, the retina must be removed [16]. As a result, to use a morphological characteristics closure procedure, the precompiled image will be separated to expand the borders and brighter sections. The luminance margins of circular objects are then detected using a clever edge detection algorithm. Furthermore, to fragment the detected circle retinal disc from of the segmented images, the circular Hough transform (CHT) is applied. The part of the eye to be removed is the circular with largest dimension. Figure 3 depicts the OD fragmented picture.

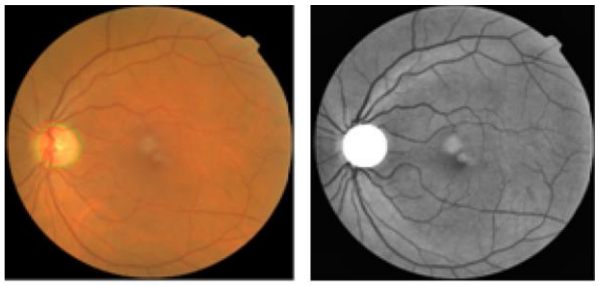

Figure. 3 Recognition of OD (leftward) and OD segmented picture (rightward)

2.4. Identification of candidates

Because the greens stream contains more details concerning red tumors, we must recover the green stream from classification stage. Then, with quantity σ set to 0.5, a Texture feature is used to improve the image quality. The standard error of a Probability function σ can be adjusted associated with the input object's ambient noise. Subsequently, the normalised picture is subjected to linguistic structures including such dilation and erosion. The comprehensive or signifier picture (GM) is created by subtracting the degraded picture from of the OD segmentation process. The MA tumors, neurons, and several noisy pixel are highlighted in the picture GM [16]. To obtain a basic picture of GM, the thresholds criterion is used. Depending just on level of noise estimating uncertainty, the threshold (Th) for intensity values is set to 0.25. The particles with the lowest SD are classified as noisy image as σ_n. Figure 4 shows the steps for extracting MA candidates.

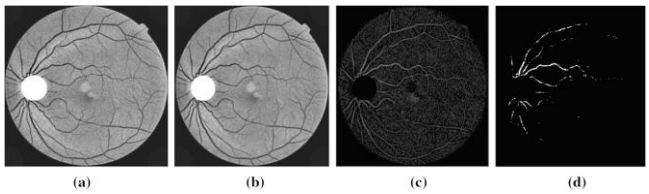

Figure. 4 Procedure in candidate removal: a) Dissimilarity augmentation, b) Morphologic renovation, c) Morphologic inundating, d) Thresholding

2.5. Retrieval of features

In MA recognition and prevention, the extraction of features phase is critical. Although LBP [17] may create a texture feature, it can also assist in the selection of MA different classifiers. The discrepancy here between centre pixel P_{Cent} as well as the neighbouring pixel P_{Neig} is initially assessed. Furthermore, the cutoff constraint is used to obtain the original image's numeric code. The data type numbers collected are then translated to numeric values. Depending on the co-occurrence matrices, those numeric values generate a 256-dimensional feature representation. A distribution of MA target region encompassing MA images and vascular images is shown in Figure 5. 256 features were extracted all along horizontal line and the matching characteristics in the co-occurrence matrices are obtained all along vertical line inside the LBP spectrum. The cross pixels are represented from each bar. The feature extraction again for MA location is the amount of cross pixels that occurs once, whereas the representation for the retinal image location is the amount of cross pixels that occurs multiple times. Every MA person's statistical distribution will be different. Especially contrasted to the generalised rotatable consistent LBP result of activities in [18] this technique is less difficult. Ultimately, the values are sent from the classification, which uses them to identify MA tumors inside the incoming test dataset.

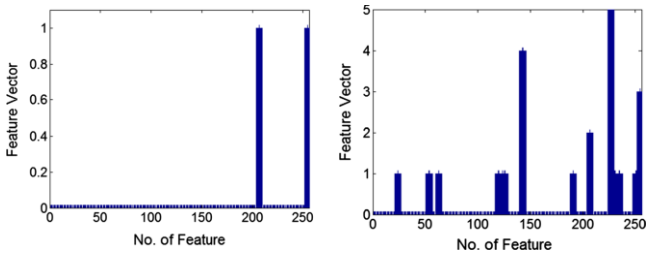

Figure. 5 Histogram of MA affected area (leftward); Histogram of vessel area (rightward)

2.6. Logistic regression

Incidentally, logistic regression is a binary classifier instead of a linear regression. For bitwise and sequential text categorization, stochastic regression is a simple and also more convenient approach. It's a classification technique that's simple to implement and delivers excellent results with binary classification categories. In the industrial world, it is a widely used categorization method. Such as the Adaboost and recurrent neural networks, the logistic regression method is a mathematical technique for classifier that can be adapted to text categorization [19]. Artificial intelligence and machine supports multi-classification tasks with a high performance variant of logistic regression framework. Logistic regression, like linear models, creates an analysis of the relationship among several parameters. Whenever the parameter to also be evaluated is a possibility on a linear ranging from zero to 1, logistic regression is appropriate in figure 6.

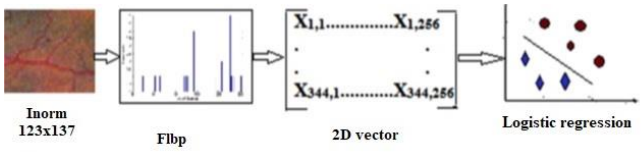

Figure. 6 Representation of classification by means of logistic regression.

3. Outcomes and discussion

Three available databases are utilised to evaluate the suggested technique's effectiveness in optic disc: ROC [20], DIARETDB1, and MESSIDOR [21]. The surface descriptors are only supplied for 50 trained photos in the ROC database, therefore only 25 pictures were used for validation and the balance for supervised learning. The accessible 1200 retina pictures in the MESSIDOR database are divided into four grade levels: DR0, DR1, DR2, and DR3. The severity is determined by the presence of MA tumors, haemorrhages, and secretions. There seem to be 546 photographs with no indications of DR, whereas the rest 654 images contain all indicators of DR.

Because 40 of a 654 photos have just MAs, a fresh database with 40 pictures with such a pixels per inch of 1388 876 is created. It is now adequate to analyze the 40 photos listed previously. In furthermore, we used the DIARETDB1 database to evaluate our approach, which contains 19 trained and 20 test photos containing MA indications. Either lesion-based assessment and picture assessment have indeed been selected for examination. Because sensitivity only can also be used to evaluate MA identification, Neimeijer et al. [22] developed a global sensing metric termed FROC rating. The FROC index is determined by graphing sensitivities on the vertical plane and the mean rate of false positives per images (FPPI) on the horizontally. An aggregate of sensitivity at 7 distinct points, like 1/8, 1/4, 1/2, 1, 2, 4, and 8 FPPI, is used to calculate the result. Receiver operating characteristics (ROC) are calculated by adjusting Th among 0 and 1 to examine per assessment. For multiple datasets, operating principles including as sensitivities, selectivity, and AUC are often examined. In ROC, 10 of the 25-image registration show no symptoms of DR,

while the other 15 pictures are accused of having 273 actual MAs. Only 27 tumors are falsely labeled in a maximum of 273 presumptive MAs, according to tests with suggested scheme. As a result, we attained an overall FPPI of 40.12 with a sensitivity of 94.58 percent in our research. Conversely, inside the MESSIDOR database, 10 of the 20 test photos show no symptoms of DR, whereas the rest 10 images are alleged to have committed 312 actual MAs. The overall FPPI after adoption is 33.11, with a sensibility of 95.83 percent. Success is usually reported accurate on structure characteristics in the different literature addressed, although in our methodology, we obtained a FROC value of 0.419, which is really the highest performance amongst findings in [15, 23–27].

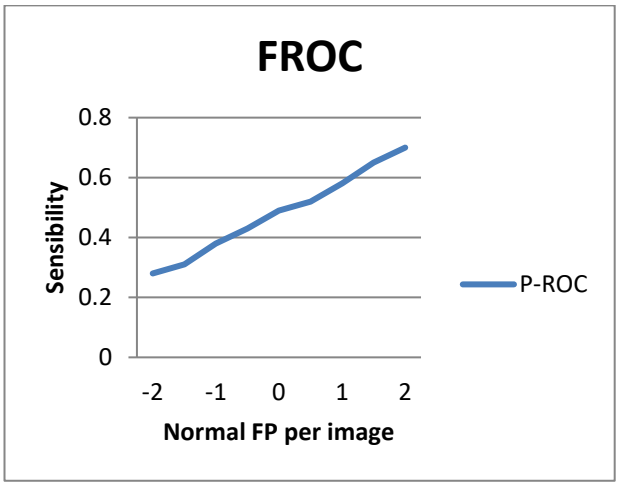

Figure. 7. FROC Curves for ROC

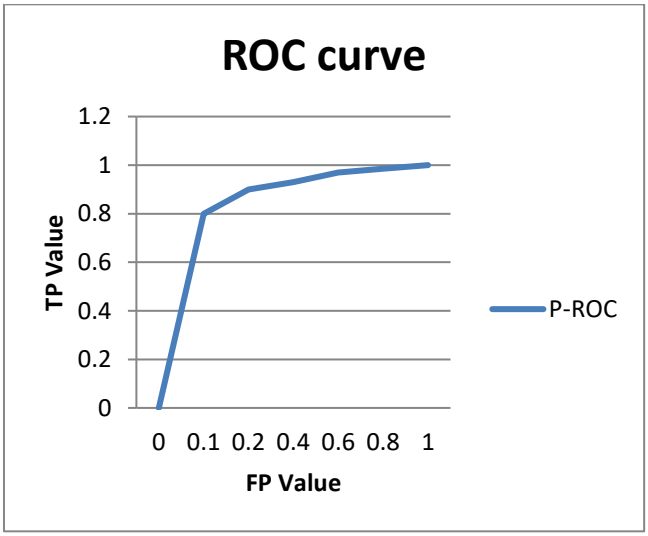

Figure 8. ROC Curves for Dataset

Comparative assessment of F-scores for advanced methodologies specified by sensitivity and FPPI. Unlike other automatic systems [24, 28, 29] this technique does not require vascular separation prior to categorization. The MA characteristics are obtained to effectively differentiate among MAs and vascular zone, as texture-based object recognition is preferable. Even though the current approach delivers satisfactory results for per injury assessment, it is necessary to examine per image processing applications. For the MESSIDOR database, the current technique had an AUC of 0.916, sensitivity of 95.83 percent, and specificity of 80 percent when diagnosing MA lesions. In the case of the ROC dataset, an AUC of 0.906 was obtained with a sensitivity of 94.58 percent and a specificity of 80 percent. Furthermore, for the DIARETDB1 dataset, we got a sensitivity of 93.93 percent and selectivity of 82 percent with only an AUC of 0.899. The FROC and ROC curves for the ROC, MESSIDOR, and DIARETDB1 datasets are shown in Figure 7 and 8. Additionally, the data demonstrate indicate our proposed technique plays best for photos with different resolutions and pictures with a variety of DR problems. Figure 9 shows a typical outcome of suggested MA identified tumors on a retinal picture. The entire computing duration is 36 seconds; however, it can take up to 50 seconds associated with the input picture quality. The average recognition period for a picture with a dimension of 1000–2000 images is 23 seconds.

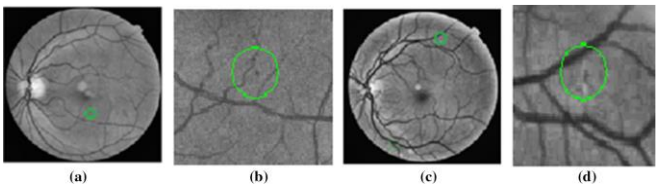

Figure. 9 a) Identify laceration in ROC model, c) Identified laceration in MESSIDOR model, b), d) Inflamed ROI

4 Conclusion

This research is a sincere attempt to locate MAs in retinal fundus photos. A second-order quantitative LBP approach is employed to lessen the complication of MA identification. The suggested technique is evaluated using three retinal vessel datasets: ROC, MESSIDOR, and DIARETDB1. With an AUC of 0.916, this approach had a sensitivity of 95.83 percent and a selectivity of 80 percent. For the MESSIDOR dataset, the proposed technique produced an F-score of 0.419 when contrasted to the FROC graphs. MA identification is more sensitive with histogram-based image retrieval than with convergences and colour scheme characteristics. On per tumor and per picture assessment, the suggested approach exhibited greater sensitivity. Based on the future outcomes, additional image retrieval stage adjustments are required to increase algorithmic effectiveness and decrease computing time. A computerized method competent of detecting any phase of DR is required to assist and boost ophthalmologists' competence. As a result, we want to expand our method in the upcoming to address the issues of detecting either haemorrhage and secretions.

Conflicts of interest

The authors declare no conflicts of interest.

References

[1] Jee D, Lee WK, Kang S. “Prevalence and risk factors for diabetic retinopathy: the Korea National Health and Nutrition Examination Survey 2008-2011”. *Invest Ophthalmol Vis Sci*, vol.54, pp. 6827–6833, 2013.

[2] Masliza H. Mohd Ali, Nani Draman, Wan M.I.W. Mohamed, Azhany Yaakub, Zunaina Embong, “Predictors of proliferative diabetic retinopathy among patients with type 2 diabetes mellitus in Malaysia as detected by fundus photography”, *Journal of Taibah University Medical Sciences*, Vol. 11, No. 4, pp. 353-358, 2016.

[3] American Diabetes Association, Diagnosis and classification of diabetesmellitus, Diabetes Care 47 (2014) S81–89.

[4] Zubair M, Malik A, Ahmad J. “Study of Plasmid mediated Extended Spectrum Beta Lactamase producing Strains of Enterobacteriaceae, Isolated from Foot Infections in North Indian tertiary care hospital”. *Diabetes Technology and Therapeutics*, vol. 12, no .4, pp. 315-324, 2012.

[5] Rui Zheng, Lei Liu, Shulin Zhang, Chun Zheng, Filiz Bunyak, Ronald Xu, Bin Li, and Mingzhai Sun, "Detection of exudates in fundus photographs with imbalanced learning using conditional generative adversarial network," *Biomed. Opt. Express*, vol. 9, pp. 4863-4878, 2018.

[6] Giji Kiruba and Benita. "Energy capable clustering method for extend

the duration of IoT based mobile wireless sensor network with remote nodes" *Energy Harvesting and Systems*, vol. 8, no. 1, pp. 55-61, 2021.

[7] Shukla R, Gudlavalleti MV, Bandyopadhyay S, Anchala R, Gudlavalleti AS, Jotheeswaran AT, Ramachandra SS, Singh V, Vashist P, Allagh K, Ballabh HP, Gilbert CE. "Perception of care and barriers to treatment in individuals with diabetic retinopathy in India: 11-City 9-state study". *Indian J Endocrinol Metab*. Vol. 20, pp. S33–S41, 2016.

[8] Manisha Verma, Bala Subramanian Raman, "Local neighborhood differencepattern: a new feature descriptor for natural and texture image retrieval", *Multimed. Tools Appl.* Vol. 77, no. 10, pp. 11843–11866, 2018.

[9] Sarni Suhaila Rahim, Vasila Palade, James Shuttleworth, Chrisina Jayne, "Automatic detection of Microaneurysms in color fundus images for diabeticretinopathy screening", *Neural Comput. Appl*. Vol .27, no. 5, pp. 1149–1164, 2015.

[10] Roberto Rosas-Romero, Jorge Martinez-Carballido, JonathanHernandez-Capistran, J. Laura, Uribe-Valencia, "A method to assist in the diagnosis of early Diabetic Retinopathy: Image processing applied to detection of Microaneurysms in fundus images", *Comput. Med. Imaging Graph*. Vol. 4, pp. 41–53, 2015.

[11] Elaheh Imani, Hamid-Reza Pourreza, Touka Banaee, "A fully automateddiabetic retinopathy screening using morphological component analysis", *Comput. Med. Imaging Graph*. Vol. 43, pp. 78–88, 2015.

[12] L. Seoud, T. Hurtut, J. Chelbi, F. Cheriet, J.M.P. Langlois, "Red lesion detectionusing dynamic shape features for diabetic retinopathy screening", *IEEE Trans.Med. Imaging*, vol. 35, pp. 1116–1126, 2016.

[13] Ting DS, Cheung GC, Wong TY. "Diabetic retinopathy: global prevalence, major risk factors, screening practices and public health challenges: a review". *Clin Exp Ophthalmol*, vol. 44, no. 4, pp. 260–277, 2016.

[14] Bo Wu, Weifang Zhu, Feishi, Shuria Zhu, Xinjianchen, "Automatic detection of Microaneurysms in retinal fundus images", *Comput. Med. Imaging Graph.* Vol. 55, pp. 106–112, 2016.

[15] Syed Ayaz Ali Shah, Augustinus Laude, Ibrahima Faye, Tom Boon Tang, "Automated microaneurysm detection in diabetic retinopathy using curve-lettransform", *J. Biomed. Opt.* vol. 21, no. 10, pp. 1–8, 2016.

[16] Su Wang, Hongying Lilian Tang, Lutfiah Ismail Al Turk, Yin Hu, Saeid Sanei,George Michael Saleh, Tunde Peto, "Localizing microaneurysms in fundus images through singular spectrum analysis", *IEEE Trans. Biomed. Eng.* Vol. 64, no. 5, pp. 990–1002, 2017.

[17] M.M. Habib, R.A. Welikala, A. Hoppe, C.G. Owen, A.R. Rudnicka, S.A. Barman, "Detection of microaneurysms in retinal images using an ensemble classifier", *Inform. Med.*, vol. 9, pp. 44–57, 2017.

[18] Mei Zhou, Kei Jin, Shaoze Wang, Juan Ye, Dahong Qian, "Color retinal image enhancement based on luminosity and contrast adjustment", *IEEE Trans. Biomed. Eng.* Vol. 46, no. 99, pp. 1–7, 2017.

[19] Das, D., Biswas, S.K. & Bandyopadhyay, S. "A critical review on diagnosis of diabetic retinopathy using machine learning and deep learning". *Multimed Tools Appl*, vol. 81, pp. 25613–25655 2022.

[20] Aimen Aakif, Muhammad Faisal Khan, "Automatic classification of plants based on their leaves", *Biosyst. Eng.* Vol. 139, pp. 66–75, 2015.

[21] http://webeye.ophth.ulowa.edu/roc/var/www/university of Iowa, retinopathyonline challenge: 2007.

[22] Almasi, R., Vafaei, A., Kazeminasab, E. et al. "Automatic detection of microaneurysms in optical coherence tomography images of retina using convolutional neural networks and transfer learning". *Sci Rep* vol. 12, pp. 13975, 2022.

[23] Diana Veiga, Nelson Martins, Manuel Ferreira, Joso Monterio, "Automatic Microaneurysm detection using laws texture Microaneurys msks and support vector machines, Computer Methods" *Biomechanics and Biomedical Imaging and Visualization*, 2017.

[24] Wei Zhou, Chengdong Wu, Dali Chen, Yugen Yi, Du. Wenyou, "Automatic microaneurysm detection using the sparse principal component analysis-based unsupervised classification method", vol. 5, pp. 2563–2572, 2017.

[25] Behdad Dashtbozg, Jiang Zhang, Fan Huang, Bart M. ter Haar Romeny, "Retinal Microaneurysms detection using local convergence index features", *IEEE Trans.Image Process.* Vol. 27, no. 7, pp. 3300–3315, 2018.

[26] Zhitao Xiao, Xinpeng Zhang, Lei Geng, "Automatic non-proliferative diabeticretinopathy screening system based on color fundus image", *Biomed. Eng.* vol. 16, pp. 1–19, 2017.

[27] Veena Mayya, Sowmya Kamath S., Uma Kulkarni, "Automated microaneurysms detection for early diagnosis of diabetic retinopathy: A Comprehensive review, Computer Methods and Programs" *Biomedicine Update*, Vol. 1, pp. 100013, 2021.

[28] Divakar Yadav, Arun Kumar Karn, Anurag Giddalur, Arti Dhiman, Sakshi Sharma, Muskan, Arun Kr. Yadav, "Microaneurysm detection using color locus detection method", *Measurement*, Vol. 176, pp. 109084, 2021.

[29] D. Jeba Derwin, S. Tamil Selvi, O. Jeba Singh, B. Priestly Shan, "A novel automated system of discriminating Microaneurysms in fundus images", *Biomedical Signal Processing and Control*, Vol. 58, pp. 101839, 2020.